Supporting information

Synthesis of a New Dinuclear Cu(I) Complex with a Triazine Ligand and Diphenylphosphine Methane: X-ray Structure, Optical Properties, DFT Calculations, and Application in DSSCs

Materials and Methods

General

All chemicals, such as 3-(2-Pyridyl)-5,6-diphenyl-1,2,4-triazine (L) and Bis(diphenylphosphino)methane (dppm) and $[Cu(MeCN)_4]PF_6$ were purchased from Sigma-Aldrich and used as received without further purification. Dye N719 was purchased from Solaronix. Elemental analysis was performed on an Elementar Vario ELII instrument. IR spectra were obtained using a Bruker Alpha Tensor 27 Vertex Series spectrophotometer with KBr discs in the 4000–500 cm^{-1} region. The ^{1}H and ^{31}P NMR spectra were determined with Bruker Advance III-400 spectrometer. Chemical shifts are reported in ppm and were referenced to residual solvent resonances. Uv-vis absorption spectra were recorded on a Shimadzu UV-1800 spectrophotometer. Electrochemical measurements were made using a Bio-Logic VMP-300 potentiostat/galvanostat with platinum, silver wire, and $Ag/AgNO_3$ as working, counter, and reference electrodes, respectively. Substrates were dissolved in HPLC grade CH_3CN (ca. 8×10^{-5} M) containing 0.025 M tetrabutylammonium hexafluorophosphate $(nBu_4N)PF_6$ as supporting electrolyte and a rate of 20 mVs^{-1}. Thermogravimetric analyses were performed on a TA SDT Q600 apparatus in a range of 30-800 °C (10 °C min^{-1}) using nitrogen (50 mL min^{-1}) as an inert gas.

Preparation of $[Cu_2(L)_2dppm](PF_6)_2$ (1)

To a stirring solution of [3-(2-Pyridyl)-5,6-diphenyl-1,2,4-triazine)] (L) (40 mg, 0.12888 mmol) and bis(diphenylphosphino)methane (dppm) (25.10 mg, 0.06444 mmol) in 2 mL of a 1:1 (*v*/*v*) mixture of CH_2Cl_2 and CH_3CN, $[Cu(MeCN)4]PF_6$ (48.04 mg, 0.06444 mmol) was added to obtain a dark red solution. The mixture was stirred throughout 2 h at 30 °C. Red single-crystals were obtained by vapor diffusion of diethyl ether into the concentrated solution of **1** (yield: 85.98 mg, 76%). IR (KBr, cm^{-1}): 3054 (w), 1600 (w), 1511 (m), 1479 (w), 1436 (m), 1402 (m), 1373 (m), 1305 (w), 1282 (w), 1257 (w), 1186 (w), 1143 (w), 1099 (w), 1006 (w) , 838 (s), 771 (m), 740 (m), 698 (w), 607 (m), 557 (m), 520 (w) cm^{-1}. ^{1}H NMR (400 MHz, acetone-d_6, 30 °C) δ 8.80 (d, J=8 Hz, 2H, Ar-H), 8.17 (t, J=8.00 Hz, 2H, Ar-H), 7.64 (m, 4H, Ar-H), 7.52 (m, 14H, Ar-H), 7.34 (m, 25H, Ar-H), 3.93 (t, J=8 Hz, 2H, CH_2) ppm. ^{31}P NMR (162 MHz, acetone-d_6, 30 °C) δ -7.42 (s, Ar-P), -144.67 (hept, ^{1}J = 708.47 Hz, PF_6) ppm. UV–Vis (ethanol 2 x 10^{-5} mol dm^{-3}): λ (ε: M^{-1} cm^{-1}) 286 (56700), 338 (26700), 410 (13150) nm. Anal. Calc. (%) for $C_{65}H_{50}Cu_2F_{12}N_8P_4$: C, 54.90; H, 3.54; N, 7.88. Found (%): C, 54.63; H, 3.91; N, 7.93.

Crystallography

The single crystalline X-ray diffraction study of the title complex was determined at T = 130 K in an Oxford Diffraction Gemini "A" diffractometer equipped with a CCD detector and using Mo-K_α radiation (λ = 0.71073 Å) and an Oxford Instruments Cryojet ES-75 cooler. Unit cell parameters were calculated with a set of three runs of 15 frames each (1° in ω). The double pass scanning method was used to exclude noise [1]. The collected frames were integrated using an orientation matrix resolution of the narrower frame scans. The final cell constants were obtained by global refinement. Diffraction data were corrected for absorbance through an analytical-numerical absorption correction, which employed a multifaceted crystal model based on Laue symmetry

expressions with equivalent reflections [2]. Structure resolution and refinement were performed with SHELXT-2014 [3] and SHELXL-2014 [4]. All non-hydrogen atoms were refined anisotropically. All hydrogen atoms were placed in positions calculated geometrically using the driving model. Hydrogen bonding interactions in the crystal lattice were determined with the MERCURY software package [5]. The figures were made with MERCURY [5] and DIAMOND [6].

1: $C_{65}H_{50}Cu_2F_{12}N_8P_4$, *MW* = 1422.09 g mol^{-1}, monoclinic, space group *P21/c*, *a* = 18.9916(9), *b* = 18.6701(9), *c* = 20.9494(5) Å, α = 90, β = 111.621(6), γ = 90°, *V* = 6905.5(6)Å3, *Dc* = 1.368 g cm^{-3}, *T* = 130 K, *Z* = 4, μ(MoK$_\alpha$) = 0.785 mm^{-1}. Total 38,974 reflections, 16,247 unique (R_{int} = 0.0427). Refinement of 16,247 reflections (820 parameters) with $I > 2\sigma(I)$ coverged at final R_1 = 0.0587 (R_1 all data = 0.1131), wR_2 = 0.1280 (wR_2 all data = 0.1644), *F*(000) = 2888, *gof* = 1.059. CCDC 2278925.

Solar cell construction

Material for the manufacture of dye-sensitized solar cells was purchased from Solaronix, Switzerland. DSSCs sensitized with $[Cu_2(L)_2dppm](PF_6)_2$ (1) and 1:1 mixture dye combination 1/N719 and N719 were prepared, modifying the method of Grätzel [7,8]. To prepare the working electrodes, fluorine-doped tin oxide (FTO) glass plates (Solaronix TCO30-8, 3 mm thick) were washed in a consecutive ultrasonic bath in a 1% soap solution, distilled water, and ethanol (HPLC grade) for 10 min each. Finally, the electrodes were subjected to UV light (λ = 254 nm) for 10 minutes in a peroxide solution in deionized water (5%). Subsequently, with the Deep Coating method, a compact layer of TiO_2 was added to each FTO plate by immersion in a 40 mM $TiCl_4$ aqueous solution (70 °C for 30 min), after which they were washed with distilled water and ethanol. Next, the glass plates were sintered with TiO_2 at 450 °C for 30 min in a muffle (Thermolyne SCIENTIFIC FB1410M); they were allowed to cool to room temperature and washed with ethanol. Therefore, with the Screen Print method, mesoporous TiO_2 was deposited on each FTO glass (0.2 cm^2), and finally, the sintering process was repeated. Once cooled, a second Dip Coating treatment was performed, followed by a 1-hour treatment with UV radiation (λ = 254 nm). The electrodes were immersed in 0.3 mM solutions of either **1** or N719 in a CH_3CN/tert-butanol solvent mixture (50:50% *v*/*v*) for 12 h in the dark. For co-sensitization, the electrode with **1** was immersed under the same conditions in 0.3 mM solutions of N719 in a CH_3CN/tert-butanol mixture (50:50% *v*/*v*). Notably, the amount of N719 used in the co-sensitized device was only half (50%) that of the control DSSC of N719. For the elaboration of the counter electrodes, FTO plates with 0.5 mm diameter holes on the edge of the driver's side were used. The FTO glasses were cleaned with the abovementioned procedure for the working electrodes. Accordingly, the platinum layer was deposited by screen printing on the entire surface of the FTO glass, followed by drying at 120 °C for 10 min. The plates were then immediately immersed for 1 min in a 10 mM H_2PtCl_4 solution in isopropanol and dried at 120 °C for 5 min. Finally, a heat treatment was applied at 400 °C (heating rate 1.2 °C/min) for 15 min, followed by cooling to 100 °C at a rate of 10 °C/min.

The working and counter-electrodes were joined by a thermoplastic (Meltonix 1170-25 DuPont Surlyn) of 60 μm thickness (treatment at 110 °C for ~5 min in an oven). Finally, an electrolyte composed of 0.05 M I_2, 0.1 M LiI, 0.5 M 4-tert-butylpyridine, and 0.6 M tetrabutylammonium iodide dissolved in a mixture of acetonitrile and 3-methoxypropionitrile (50:50% *v*/*v*) was introduced into the DSSCs. The remaining air was removed by vacuum treatment.

With a potentiostat/galvanostat (Bio-Logic VMP-300) and an AM 1.5 light source solar simulator (Oriel LCS-100), the performance of the DSSCs was measured by lateral irradiation of the DSSC anode. The incident light intensity was 100 mW cm^{-2} (1 sun), calibrated using a reference Silicon solar cell.

Computational detail

Hirshfeld surface analysis and complex fingerprint plots were performed from the Crystallographic Information Files (CIF) using CrystalExplorer 17 [9]. The Hirshfeld surface was mapped in the range 0.5 to +1.5 for dnorm, -4 to 0.4 in Curvedness, and Shape Index -1 to 1.

DFT analysis [10-13] for the complex was performed with the Gaussian 09 package [14] and processed with the GaussView and Swizard software [15,16]. Starting from the monocrystalline structure by diffraction, the minimum energy structures were determined by frequency calculations (without imaginary frequencies). Using time-dependent density functional theory (TD-DFT), the transitions between the different molecular orbitals [17,18] were determined using the M06 hybrid-meta-GGA functional [19] in combination with the 6-31G(d) base sets [20] for the C, H, N and P atoms and DZVP [21] for the Cu atom. The effects of a solvated environment were estimated with the integral equation formalism for the continuum polarizable model (IEF-PCM) and the implementation of the out-of-equilibrium solvation model [22,23]. The solvent used for this study was ethanol.

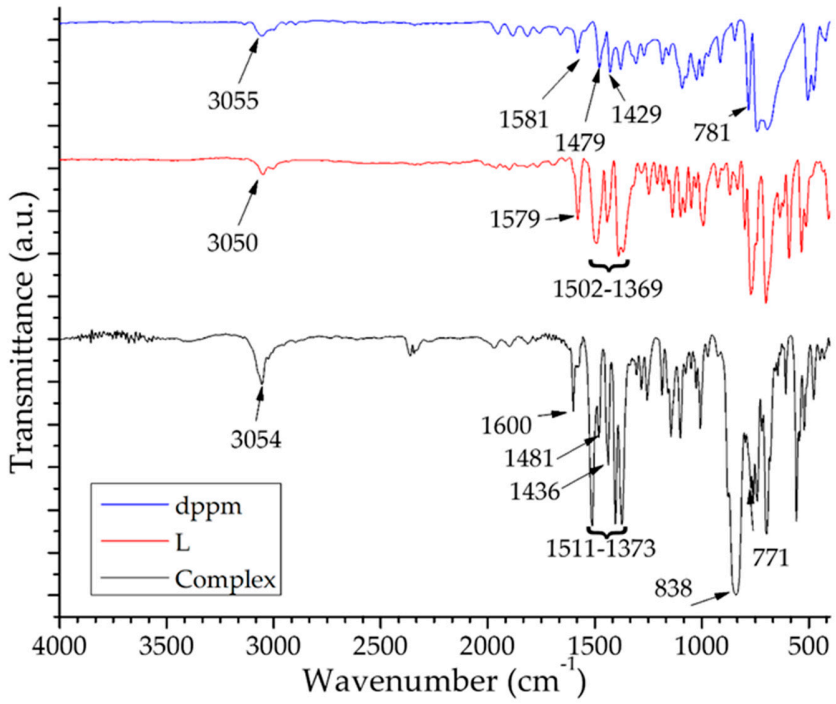

Figure S1. Infrared spectra of complex and the corresponding starting materials.

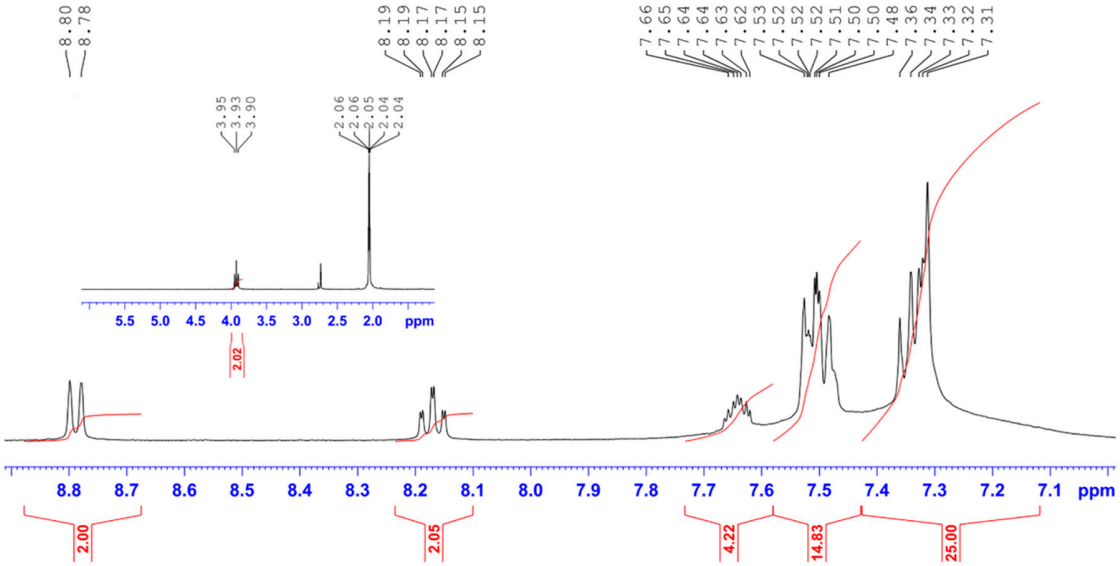

Figure S2. ^{1}H NMR spectrum of the complex in acetone-d_6.

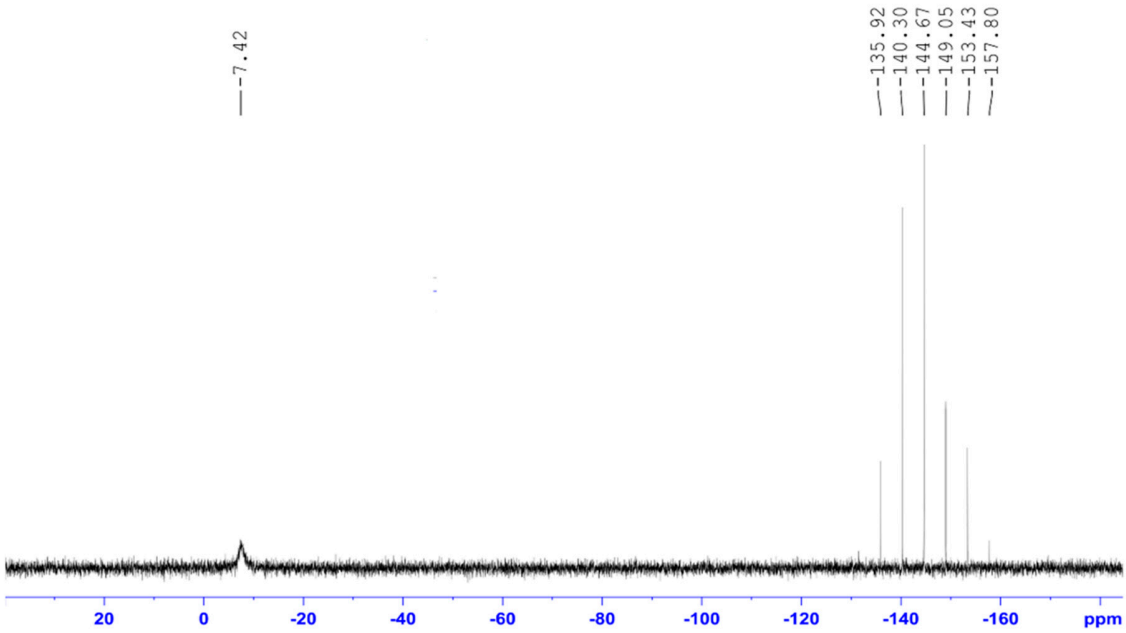

Figure S3. ^{31}P NMR spectrum of the complex in acetone-d_6.

Table S1. Geometries of intermolecular hydrogen bonds and π···π contacts in complex **1**.

D-H···A	D-H (Å)	H···A (Å)	D···A (Å)	D-H···A (°)	Symmetry codes
C62-H62···N7	0.95	2.65	3.565(6)	161	-1/2+x,-1/2+y,-1/2+z
C1-H1A···F1	0.99	2.63	3.603(6)	166	x,y,x
C8-H8···F8	0.95	2.53	3.372(8)	147	-x+1,-y+1,-z+1
C8-H8···F9	0.95	2.49	3.065(7)	119	-x+1,-y+1,-z+1
C40-H40···F7	0.95	2.63	3.582(6)	17	-x,-y+1,-z+1
C40-H40···F10	0.95	2.47	3.214(4)	135	-x,-y+1,-z+1
C46-H46···F5	0.95	2.59	3.434(7)	147	x-1/2,-y+1/2,+z-1/2
C47-H47···F2	0.95	2.57	3.323(8)	136	x-1/2,-y+1/2,+z-1/2
C49-H49···F1	0.95	2.50	3.365(8)	150	x,y,x
C61-H61···F3	0.95	2.49	3.222(6)	133	x,y,x
C63-H63···F10	0.94	2.30	3.219(6)	162	-x+1/2,+y-1/2,-z+1.5
C9-H9···π[a]	0.95	3.58	4.336	138	-x+1,-y+1,-z+1
C17-H17···π[b]	0.95	3.46	3.943	114	-x+1/2,+y-1/2,-z+1.5
C33-H33 ···π[c]	0.95	3.53	4.105	121	-x+1/2,+y-1/2,-z+1/2
π···π[d]			3.756		-x+1,-y+1,-z+1

[a] Centroid: C25, C26, C27, C28, C29, C30
[b] Centroid: C60, C61, C62, C63, C64, C65
[c] Centroid: C42, C43, C44, C45, C46, C47
[d] Centroids: N4, C5, C9, C6, C8, C7 and C5, C8, C9, C6, C7, N6

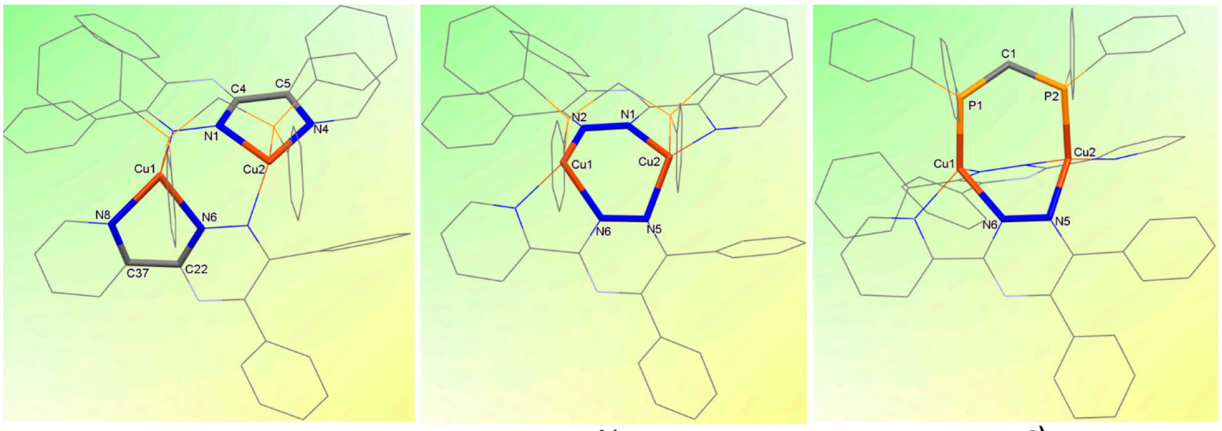

Figure S4. Perspective views of $[Cu_2(L)_2dppm]^+$ in the crystal structure of **1**, showing a) two five-membered Cu-N-C-C-N, b) one six-membered Cu-N-N-Cu-N-N and c) one seven-membered Cu-N-N-Cu-P-C-P chelate rings. Hydrogen atoms have been omitted for clarity.

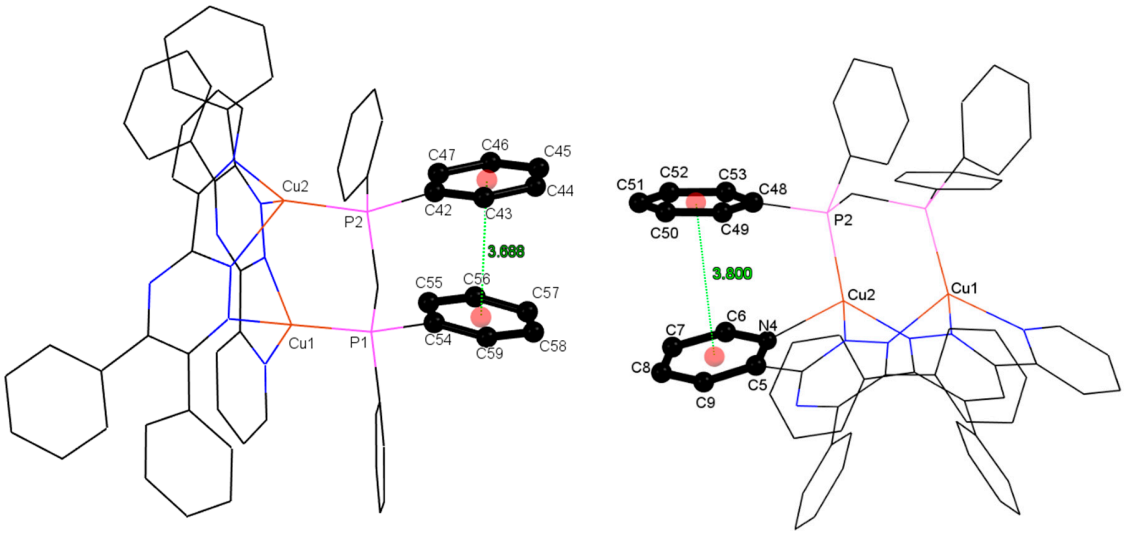

Figure S5. Intramolecular π···π interactions in the crystal structure of **1**. Hydrogen atoms have been omitted for clarity.

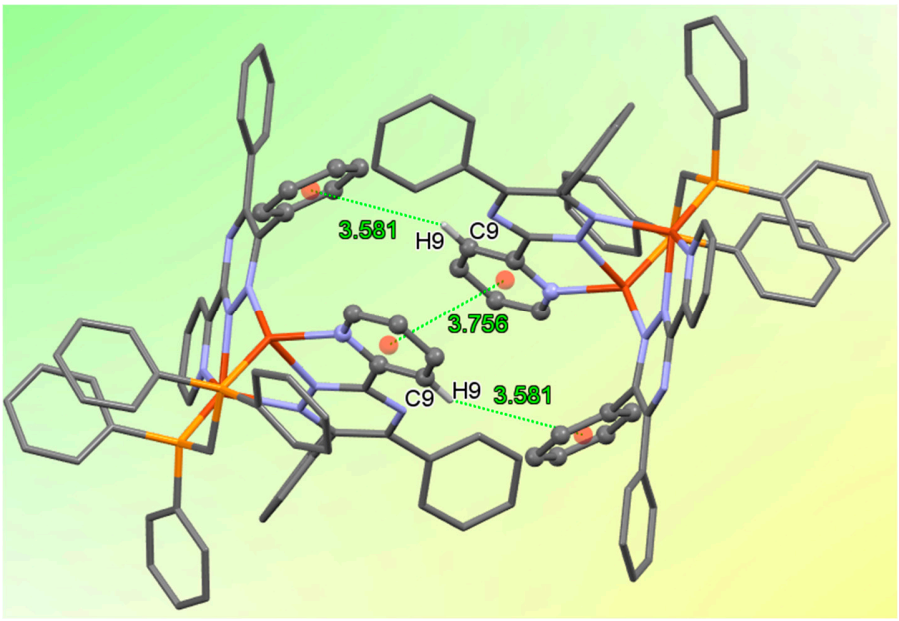

Figure S6. Intermolecular C-H··· π and π- stacking interactions between pair of $[Cu_2(L)_2dppm]^+$ cations. Hydrogen atoms have been omitted for clarity.

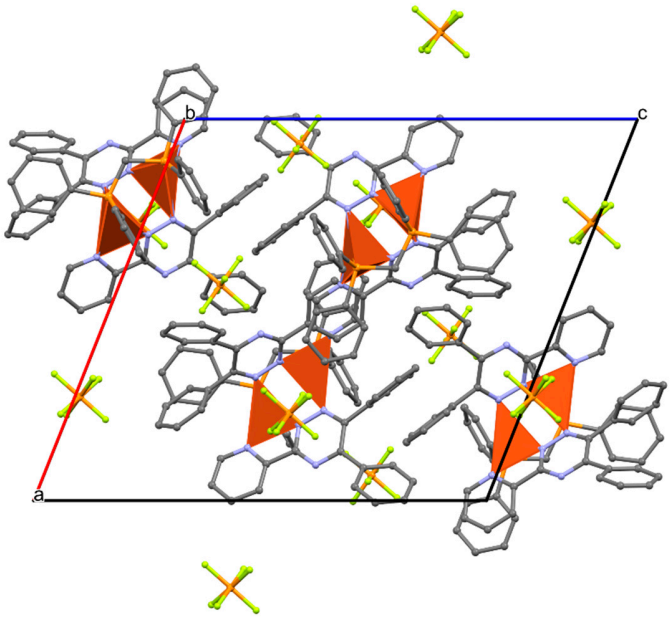

Figure S7. Perspective view of the three-dimensional (3D) hydrogen-bonded network in the crystal structure of complex **1**, formed through C-H···N, C-H···F, C-H···π and π···π interactions. Hydrogen atoms have been omitted for clarity.

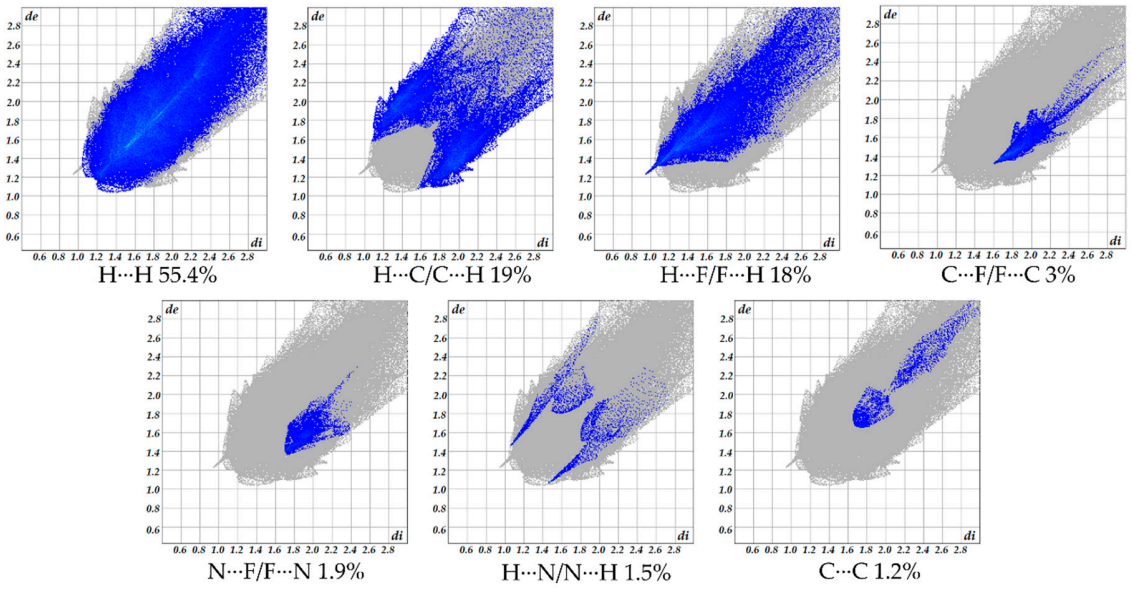

Figure S8. Percentages of intermolecular interactions in the fingerprint plot for complex **1**.

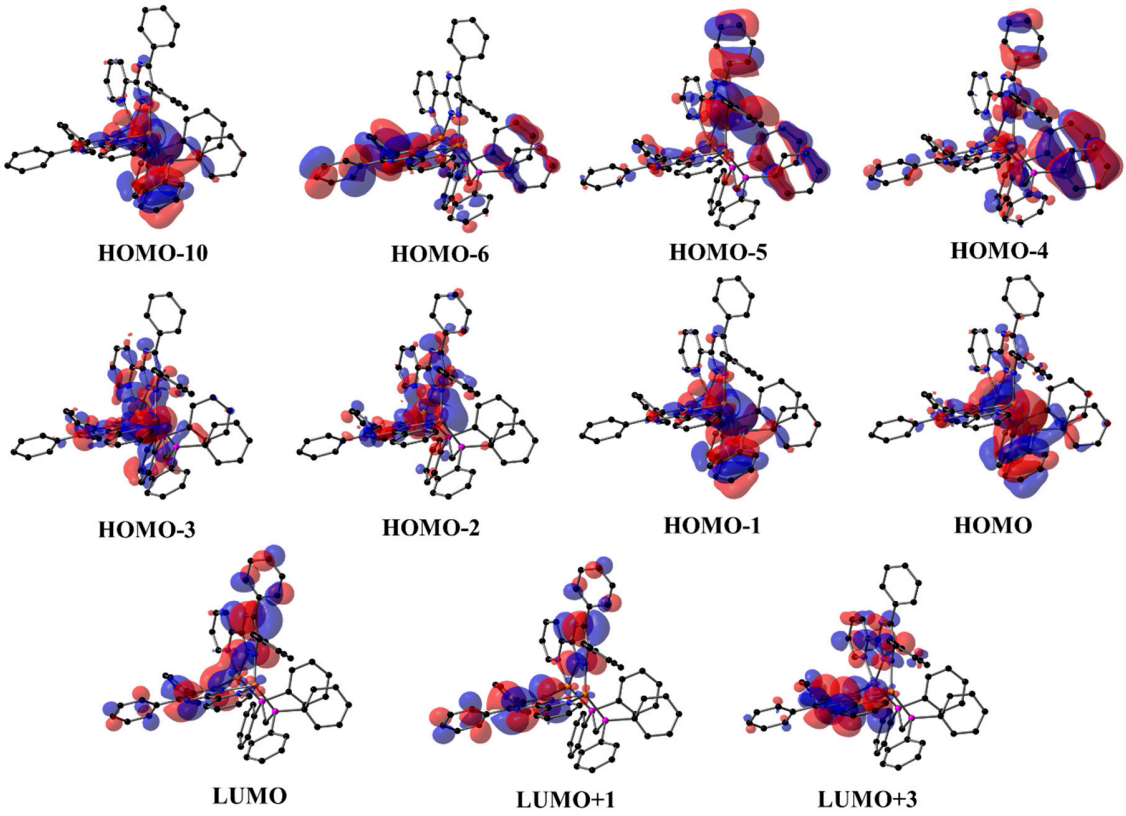

Figure S9. HOMO and LUMO frontier orbital plots of the title complex on TD-DFT calculations.

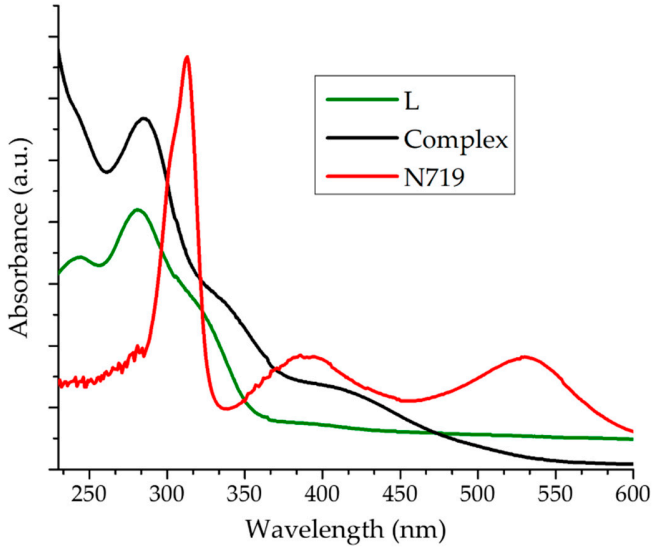

Figure S10. UV-Vis absorption spectra of complex, free ligand L and N719 recorded in $2x10^{-5}$ mol/L solution in ethanol.

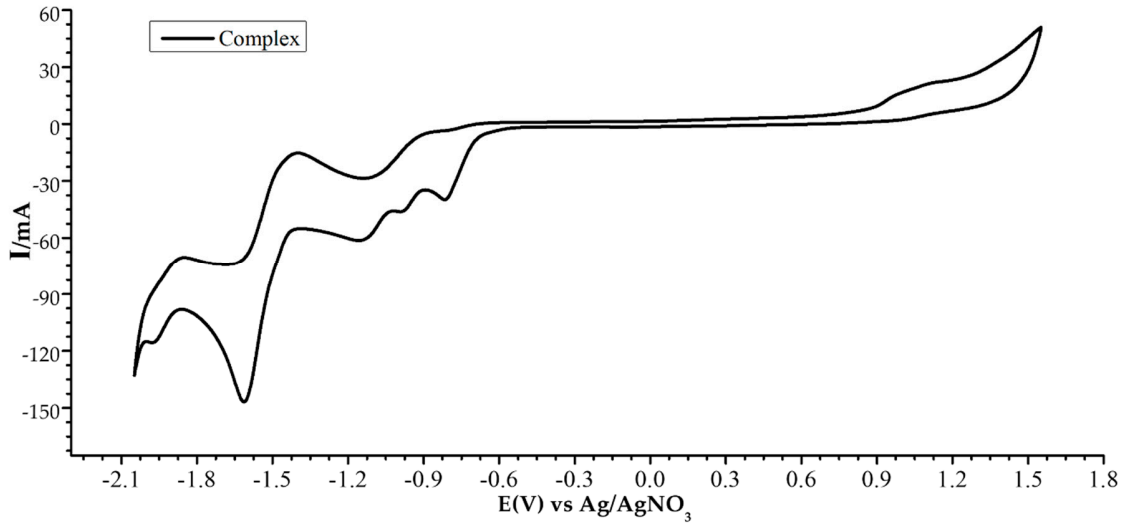

Figure S11. Cyclic voltammogram of $[Cu_2(L)_2dppm](PF_6)_2$ ($5x10^{-3}$ M) in acetonitrile at T = 298 K using NBu_4PF_6 (0.1 M) as supporting electrolyte (scan rate = 20 mVs^{-1}).

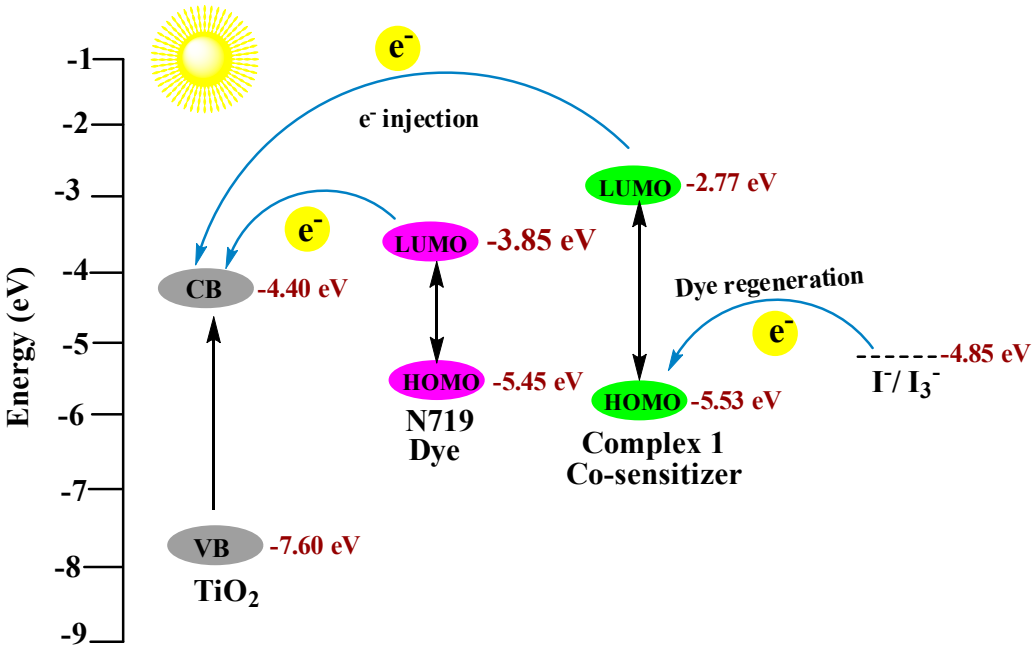

Scheme S1. Schematic illustration of the operational principle of DSSC and energy diagram of HOMO and LUMO levels for dyes compared to the energy levels for TiO_2.

References

1. *CrysAlisPro*, Version 1.171.37.35; Agilent Technologies: Yarnton, UK, 2014.

2. Clark, R.C.; Reid, J.S. The analytical calculation of absorption in multifaceted crystals. *Acta Crystallogr. Sect. A* Found. Crystallogr.**1995**, *A51*, 887–897.
3. Sheldrick, G.M. ShelXT-Integrated space-group and crystal-structure determination. *Acta Cryst.* **2015**, A71, 3–8.
4. Sheldrick, G.M. Crystal structure refinement with SHELXL. *Acta Crystallogr. Sect. C Struct. Chem*. **2015**, *C71*, 3–8.
5. Macrae, C.F.; Bruno, I.J.; Chisholm, J.A.; Edgington, P.R.; McCabe, P.; Pidcock, E.; Rodriguez-Monge, L.; Taylor, R.; van de Streek, J.; Wood, P.A. Mercury CSD 2.0—New features for the visualization and investigation of crystal structures. *J. Appl. Crystallogr*. **2008**, *41*, 466–470.
6. Brandenburg, K. *Diamond*, version 4.3.2; Crystal Impact GbR: Bonn, Germany, 2017.
7. Ito, S.; Chen, P.; Comte, P.; Nazeeruddin, M.K.; Liska, P.; Péchy, P.; Grätzel, M. Fabrication of screen-printing pastes from TiO_2 powders for dye-sensitized solar cells Prog. *Photovoltaics*, **2007**, *15*, 603-612.
8. Ito, S.; Murakami, T.N.; Comte, P.; Liska, P.; C. Grätzel, C.; Nazeeruddin, M.K.; Grätzel, M. Fabrication of Thin Film Dye Sensitized Solar Cells with Solar to Electric Power Conversion Efficiency over 10%. *Thin Solid Films*, **2008**, *516*, 4613-4619.
9. Turner, M.J.; McKinnon, J.J.; Wolff, S.K.; Grimwood, D.J.; Spackman, P.R.; Jayatilaka, D.; Spackman, M.A. *CrystalExplorer17*; University of Western Australia: Crawley, WA, Australia, 2017.
10. Hohenberg, P.; Kohn, W. Inhomogeneous Electron Gas. Phys. Rev. 1964, 136, B864–B871.
11. Kohn, W.; Sham, L.J. Self-consistent equations including exchange and correlation effects. Phys. Rev. 1965, 140, A1133–A1138.
12. Luo, C.; He, X.; Zhong, A.; Liu, S.; Zhao, D. What dictates alkane isomerization? A combined density functional theory and information-theoretic approach study. *Theor Chem Acc*. **2023**, *142*, 78.
13. Guo, Z.A.; Xian, J.Y.; Rong, L.R.; Qin, H.; Jie, Z. Theoretical study of metal ion impact on geometric and electronic properties of terbutaline compounds. *Monatsh Chem* **2019**, 150, 1355–1364.
14. Frisch, M.J.; Trucks, G.W.; Schlegel, H.B.; Scuseria, G.E.; Robb, M.A.; Cheeseman, J.R.; Scalmani, G.; Mennucci, V.B.; Petersson, G.A.; Nakatsuji, H. et al. *Gaussian 09*, Revision A. 02; Gaussian Inc.: Wallingford, CT, USA, 2009.
15. Dennington, R.; Keith, T.; Millam, J.; Eppinnett, K.; Hovell, W.L.; Gilliland, R. GaussView, version 5.0.9; Semichem, Inc.: Shawnee Mission, KS, USA, 2009.
16. Gorelsky, S.I.; Lever, A.B.P. Electronic Structure and Spectra of Ruthenium Diimine Complexes by Density Functional Theory and INDO/S. Comparison of the Two Methods. J. Organomet. Chem. 2001, 635, 187–196.
17. Stratmann, R.E.; Scuseria, G.E.; Frisch, M.J. An efficient implementation of time-dependent density-functional theory for the calculation of excitation energies of large molecules. J. Chem. Phys. 1998, 109, 8218–8224.
18. Burke, K.; Werschnik, J.; Gross, E. Time-dependent density functional theory: Past, present, and future. J. Chem. Phys. 2005, 123, 062206.
19. Zhao, Y.; Truhlar, D.G. The M06 suite of density functionals for main group thermochemistry, thermochemical kinetics, non- covalent interactions, excited states, and transition elements: Two new functionals and systematic testing of four M06-class functionals and 12 other functionals. Theor. Chem. Acc. 2008, 120, 215–241.
20. Rassolov, V.A.; Ratner, M.A.; Pople, J.A.; Redfern, P.C.; Curtiss, L.A. 6-31G* basis set for third-row atoms. J. Comput. Chem. 2001, 22, 976–984.
21. Sosa, C.; Andzelm, J.; Elkin, B.C.; Wimmer, E.; Dobbs, K.D.; Dixon, D.A. A local density functional study of the structure and vibrational frequencies of molecular transition-metal compounds. J. Phys. Chem. 1992, 96, 6630–6636
22. Scrocco, E.; Tomasi, J. Electronic Molecular Structure, Reactivity and Intermolecular Forces: An Euristic Interpretation by Means of Electrostatic Molecular Potentials. *Adv. Quantum Chem*. **1978**, *11*, 115–193.
23. Improta, R.; Barone, V.; Scalmani, G.; Frisch, M.J. A State-Specific Polarizable Continuum Model Time-Dependent Density Functional Theory Method for Excited State Calculations in Solution. *J. Chem. Phys*. **2006**, *125*, 054103.